Accepted Manuscript

Iron oxide - clay composite vectors on long-distance transport of arsenic and toxic metals in mining-affected areas

Miguel A. Gomez-Gonzalez, Mario Villalobos, Jose Francisco Marco, Javier Garcia-Guinea, Eduardo Bolea, Francisco Laborda, Fernando Garrido

PII: S0045-6535(18)30117-6

DOI: 10.1016/j.chemosphere.2018.01.100

Reference: CHEM 20681

To appear in: *ECSN*

Received Date: 26 October 2017

Revised Date: 15 January 2018

Accepted Date: 22 January 2018

Please cite this article as: Gomez-Gonzalez, M.A., Villalobos, M., Marco, J.F., Garcia-Guinea, J., Bolea, E., Laborda, F., Garrido, F., Iron oxide - clay composite vectors on long-distance transport of arsenic and toxic metals in mining-affected areas, *Chemosphere* (2018), doi: 10.1016/j.chemosphere.2018.01.100.

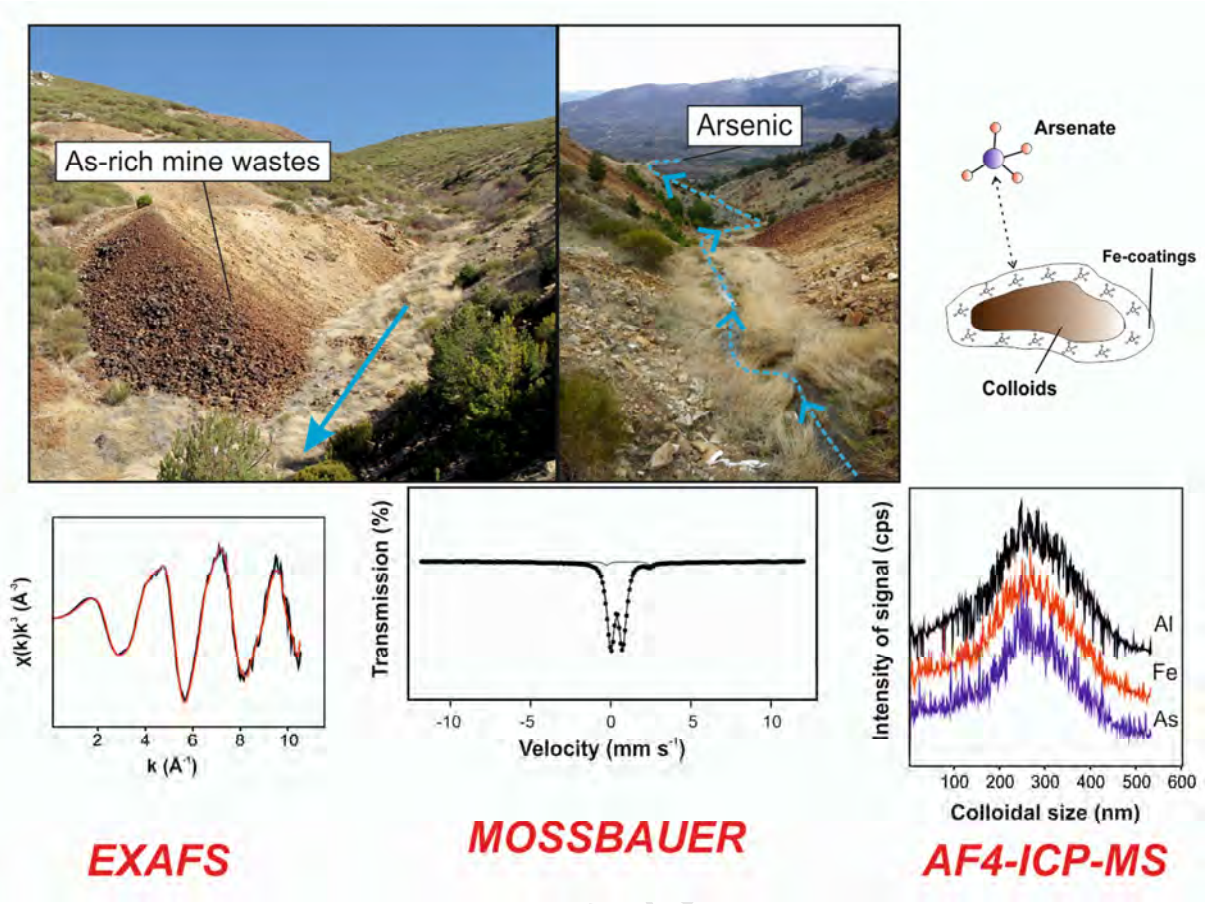

Iron oxide - clay composite vectors on long-distance transport of arsenic and toxic metals in mining-affected areas

Miguel A. Gomez-Gonzalez [a,1], Mario Villalobos [b], Jose Francisco Marco [c], Javier Garcia-Guinea [a], Eduardo Bolea [d], Francisco Laborda [d], Fernando Garrido [a*]

[a] *Museo Nacional de Ciencias Naturales (MNCN, CSIC). C/ Jose Gutierrez Abascal 2, 28006, Madrid, Spain.*

[b] *Instituto de Geología. Universidad Nacional Autónoma de México (UNAM), Coyoacán, D.F. 04510, Mexico.*

[c] *Instituto de Química Física-Rocasolano (CSIC), C/ Serrano 119, 28006, Madrid, Spain.*

[d] *Instituto Universitario de Ciencias Ambientales (IUCA), Universidad de Zaragoza. C/ Pedro Cerbuna 12, 50009, Zaragoza, Spain.*

Keywords: Arsenic; colloids; XAS; AF4-ICP-MS; mine residues; Fe-coatings

Capsule: This study indicates that nano-ferrihydrite may mobilize arsenic as mineral coatings on the surface of clay minerals. This demonstrates the role of iron coatings as arsenic scavengers and potential vector.

*corresponding author: fernando.garrido@mncn.csic.es

[1]current address: Department of Materials and London Centre for Nanotechnology, Imperial College London. Exhibition Road. London, SW7 2AZ, UK

ABSTRACT

Mine wastes from abandoned exploitations are sources of high concentrations of hazardous metal(oid)s. Although these contaminants can be attenuated by sorbing to secondary minerals, in this work we identified a mechanism for long-distance dispersion of arsenic and metals through their association to mobile colloids. We characterize the colloids and their sorbed contaminants using spectrometric and physicochemical fractionation techniques. Mechanical action through erosion may release and transport high concentrations of colloid-associated metal(oid)s towards nearby stream waters, promoting their dispersion from the contamination source. Poorly crystalline ferrihydrite acts as the principal As-sorbing mineral, but in this study we find that this nanomineral does not mobilize As independently, rather, it is transported as surface coatings bound to mineral particles, perhaps through electrostatic biding interactions due to opposing surface charges at acidic to circumneutral pH values. This association is very stable and effective in carrying along metal(oid)s in concentrations above regulatory levels. The unlimited source of toxic elements in mine residues causes ongoing, decades-long mobilization of toxic elements into stream waters. The ferrihydrite-clay colloidal composites and their high mobility limit the attenuating role that iron oxides alone show through adsorption of metal(oid)s and their immobilization in situ. This may have important implications for the potential bioavailability of these contaminants, as well as for the use of this water for human consumption.

1. INTRODUCTION

Current mines are typically designed to mitigate potential environmental impacts. However, waste dumps and tailings are common leftovers from discontinued mines (Courtin-Nomade et al., 2016). Abandoned mine wastes originally containing high sulfide concentrations are of particular concern as they become active and harmful point sources of As and other metals. Chronic exposure to low/moderate inorganic As from drinking water has been associated with increased cardiovascular mortality (Medrano et al., 2010). Knowledge of the mechanisms of contaminant release, mobility, and natural attenuation is crucial to minimize the consequences associated with mine wastes, or to devise remediation strategies.

Although As can be naturally attenuated in mining environments by associating to iron (hydr)oxides or hydroxy-sulfates, or by precipitating as scorodite ($FeAsO_4 \cdot 2H_2O$) (Courtin-Nomade et al., 2016) and other metal arsenates (Villalobos et al., 2010), colloidal particles of these minerals may be released from mining wastes and act as As carriers in surface runoff (Gomez-Gonzalez et al., 2016). Colloid-associated As may be transported and reach geochemical conditions that are different from those at the source (e.g., higher pH) thus promoting its release and bioavailability. Accordingly, none of these natural As scavengers could be considered as completely effective trapping systems in contact with flowing water because of their small particle sizes (except perhaps jarosites) (Doucet et al., 2007). This association of As to mineral colloids is important for the transport of this element in the environment and differs from the mobility behavior of both dissolved phases and of larger As-containing particles. Co-transport of contaminants by colloids has been recognized as an efficient mechanism of trace metal and organic chemical mobility (Kretzschmar et al., 1999), but little attention has been paid to As speciation in the actual mobile colloidal particles (Bauer and

Blodau, 2009) and to the As partitioning between colloids and dissolved fractions (Serrano et al., 2015).

Asymmetric flow field-flow fractionation (AF4) has been used to separate and characterize mobile colloids from natural samples (Bolea et al., 2010; Laborda et al., 2011; Baalousha et al. 2011). The mild separation conditions in absence of stationary phases contribute to the preservation of the original colloid size distribution and it can be coupled to an ICP-MS to obtain the elemental composition of the colloidal phases (Neubauer et al., 2013). Direct insight into the speciation of colloidal As and Fe can additionally be gained using X-ray absorption spectroscopy (XAS), which has been used to assess the As and Fe speciation in natural samples (O'Day et al., 2004: Voegelin et al. 2007; Chen et al. 2009) including dispersible soil colloids (Serrano et al., 2015). Recently, Gomez-Gonzalez et al. (2016) combined both techniques to demonstrate that the mineral nature of the dispersible colloidal fraction obtained after leaching scorodite-rich mine residues and sediments (Serrano et al., 2015) were similar to those colloids released by simulated rainfall experiments performed in the field. Both scorodite and Fe(III)-oxyhydroxides were identified as mineral carriers that can transport As long distances from the source.

Although the role of Fe-oxide nanoparticles as carrier phases has received attention (Bauer and Blodau, 2009; Kretzschmar et al., 1999), composite mineral colloidal assemblages may have an important role in the transport of metal(loid)s in the soil-water system, but they have scarcely been investigated. In this study, we determine the As solid-phase speciation in the dispersible (i.e., potentially detachable and mobile, <1000 nm) colloid fraction of soils along the stream that collects drainage from mine residues. The mineral phases and colloidal vectors involved in the As mobilization have been characterized and compared to the As-bearing phases present in the bulk

(i.e.<2mm) fraction of the soils. We propose a combined approach involving spectrometric and fractionation techniques to gain information on the size-dependent elemental composition of colloids, the nature of the colloidal carrier phase, and the speciation of the associated contaminants.

2. EXPERIMENTAL

2.1. Site description, sample collection and analyses

The experiment was conducted along a stream gorge (NW Madrid, Spain) that collects water drainage from an abandoned mine in the Guadarrama mountain-range (40º52'04.48" N - 3º43'48.68" O, 1475 meters altitude), where metal(oid) contamination had been previously reported (Moreno-Jiménez et al., 2009). Massive pyritic residues (~500 m^2 of surface, 3 meter-thick, 22 g kg^{-1} of As) remain on the soil surface and are subjected to weathering and erosion. There, 0-15 cm depth bulk samples were taken from (1) the arsenic-bearing waste-pile (WP), (2) four sampling points located at 28, 190, 410 and 815 m away from the WP along the gorge downstream (A-B-C-D, respectively), and (3) adjacent to a semi-permanent water course (Figure S1). Additional undisturbed soil cores (5-cm diameter, 15-cm depth) were collected from the downstream locations (A-B-C-D) and kept under anoxic conditions. Stream water samples were collected from the exit of the abandoned mine (WP) and near the sampling locations. All samples were processed as described in the Supplementary Material (SM) where the main physicochemical properties are presented (Tables S1, S2a-b, S4). Additional observations and analyses were performed through environmental scanning (ESEM) and transmission electron microscopy (TEM).

2.2. Isolation of dispersible colloidal and dissolved fractions

The maximum amount (mg kg^{-1} soil) of potentially releasable colloids from the samples was termed 'dispersible colloidal fraction' (DCF, ≤ 1000 nm) (Serrano et al., 2015). Two other fractions were isolated from the DCF upon ultrafiltration through 10 nm pore-size membranes: (i) the solid colloidal fraction (CF, 1000-10 nm) deposited onto the ultrafiltration membrane and (ii) the truly water soluble or dissolved fraction (DF, <10 nm) that passed through membranes. The experimental procedure is described in the SM.

DCF aliquots were used for AF4-ICP-MS and TEM analyses, Mössbauer spectroscopy, and for colloidal mass and element quantification. Aqueous As and metal concentrations in the dissolved fraction (DF) were quantified by ICP-MS and the colloidal fraction (CF, 1000-10 nm) obtained upon ultrafiltration was analyzed by As and Fe K-edge XAS spectroscopy (Figure S2).

2.3. Size characterization and element quantification by AF4–ICP-MS

The DCFs from A-B-C-D were analyzed by AF4 (AF2000, *Postnova Analytics*) with a coupled UV-Vis diode array detector (*Shimadzu*, wavelength range: 200-650 nm). The AF4-UV-Vis system was coupled to an ICP-MS (ELAN DRC-e *Perkin Elmer*) to perform an on-line multi-element quantification. The instrumental conditions of the AF4-UV-Vis-ICP-MS system were previously tested (Serrano et al., 2015) and are described in the SM.

2.4. As and Fe K-edge X-ray absorption spectroscopy (XAS) analyses

Arsenic and Fe XAS measurements were done on bulk (<2 mm) soil samples and on their CF (1000-10 nm). EXAFS spectra were recorded at the BM25A beamline (ESRF,

France) (6 GeV, 100 mA, Si(111) monochromator crystals) at room temperature using a 13-element Ge(Li) solid-state detector. The spectra were obtained by averaging 5-7 replicate scans. Both soil and CFs from A to D sampling points were transported under anoxic conditions and measured inside a vacuum chamber to preserve the original As and Fe speciation. Reference and sample spectra were analyzed by linear combination fitting (LCF) using the code Athena (Ravel and Newville, 2005). Details about the XAS spectra collected, LCF analyses, and reference spectra are shown in the SM.

2.5. Mössbauer spectroscopy analyses

Room temperature ^{57}Fe Mössbauer data of both bulk and colloidal samples were recorded in transmission mode using a conventional constant acceleration spectrometer and a ^{57}Co(Rh) source, analyzing ~200 mg of each sample previously powdered and capsuled in polyvinyl chloride (PVC) holders which ensures an effective thickness of 5-10 mg Fe cm^{-2} per sample. The velocity scale was calibrated using a 6 μm-thick α-Fe foil. The isomer shifts were referred to the centroid of the spectrum of α-Fe. The fitting hyperfine parameters are summarized in Table S7.

3. RESULTS

3.1. Bulk soil sample characterization

3.1.1. Physicochemical properties and metal(oid) concentrations

The WP shows high electrical conductivity (EC, 237 μS cm^{-1}), low pH (3.5) and total organic carbon (TOC) (0.2%) in comparison with the downstream samples (A, B, C, D) which presented circumneutral pH, EC in the range 19-55 μS cm^{-1} and TOC values from 1.5-5.5% (Table S1).

All samples contained quartz and albite as principle minerals in the <2-mm fraction (Table S2a). Their <2-μm fractions (Table S2b) were dominated by montmorillonite and jarosite in the WP, and by illite, and either kaolinite, or microcline and albite in the downstream soils.

The As, Fe and Pb pseudo-total concentrations were highest in the WP and decreased with distance from the contamination focus (Table 1). Conversely, Al, Mn and Zn concentrations were lowest in the WP but they also decreased with distance starting from point A downstream. This could be the result of the enhanced mineral acidic dissolution at the WP and the subsequent element enrichment at the closest point (A).

3.1.2. Element fractionation in solid phase: Sequential extraction procedure

Common to all samples is the absence of bioavailable, or exchangeable, As (step I) (Table S4). In the WP, 74% of the total As was extracted in step IV (targeting poorly crystalline Fe-oxyhydroxides). Riverbed soils showed different As solid phase distribution than the WP. The fraction of As extracted from step II (strongly adsorbed complexes) was similar in samples A and B (~22% of total As) but decreased at the farthest distance from the WP (point D). The As extracted in step III (amorphous Fe hydroxides, carbonates and volatile sulfurs) represented on average 20% of the total amount in samples A and C but decreased to 9% in point D. The As fraction extracted from step IV decreased downstream from 26% to 13% of the total As content. Conversely, the fraction of As associated to crystalline Fe-oxyhydroxides increased with distance to the WP from 8% to 33% and 25% in samples C and D, respectively. The farthest sample from the WP (D) showed a significant contribution of residual fraction (40%).

198 Iron was mostly extracted in steps III (32%) and IV (24%) (amorphous and weakly
199 crystalline Fe-oxyhydroxides, respectively) in the WP. The riverbed soils showed a
200 large residual Fe fraction from 23% (B) to 74% (D). Similarly, Al was mostly extracted
201 in step III, varying from 20% (WP) to 64% (C). Similar to Fe, sample D stood out for
202 the amount of Al in the residual fraction (43%), but residual Al was also high in the WP
203 (61%) (Table S4).
204
205 *3.1.3. Observations and analysis through scanning electron microscopy*
206 The WP was characterized by As-Ag-bearing mineralized veins of quartz that also
207 contained silica and Fe-oxides together with primary sulfide and sulfosalts such as
208 arsenopyrite, pyrite and scorodite (Figure S3a-b). Large quartz and feldspar grains were
209 abundant in samples downstream. Arsenic was found associated to Fe-oxyhydroxides
210 showing low As/Fe concentration ratios by EDX in selected particles (Figure S3c-d-e).
211 The EDX indicated the highest As/Fe ratio in the WP sample, while downstream
212 samples presented decreasing As content with distance to the contamination focus. In
213 sample D (Figure S3f), organic microparticles with important Mn and As content were
214 detected.
215
216 *3.1.4. Speciation of Fe-mineral phases: Mössbauer spectroscopy*
217 All Mössbauer spectra were dominated by an intense paramagnetic doublet whose
218 parameters can be associated to Fe(III) in octahedral oxygen coordination (Maddock,
219 1985), and by a less intense second doublet corresponding to Fe(II)-octahedral (Figure
220 S6).
221 Iron content in the WP was mainly Fe(III), 16% of whose total content corresponded to
222 goethite and 81% to a Fe(III)-illite/Fe(III)-(hydr)oxides mixture, other than goethite

(Table S7). From the WP downstream, the ratio Fe(II)/Fe(III) was lowest in sample A (0.14), increased to 0.27 in sample B, but decreased to 0.18 in in sample D (Table 2). Minor presence of hematite was detected in points C and D.

3.1.5. As speciation of bulk soils: X-ray absorption spectroscopy

Linear combination fitting (LCF) analyses of As spectra, acquired in anoxic conditions, indicated the adsorption of As on Fe(III)-oxyhydroxides, such as ferrihydrite and goethite (Table 3, Figure 1). Also, significant contributions of scorodite (26%) and As-jarosite (17%) were found in the WP.

3.2. Characterization of the colloidal fraction of contaminated soils

3.2.1. Colloid-mass and metal(loid) quantification

All soil samples released a larger mass of colloids than the WP (Table 4b). Colloidal mass in the DCF varied little from A (~9200 mg kg^{-1}) to D (~7900 mg kg^{-1}). The As colloidal concentration of the samples decreased from ~10000 mg kg^{-1} in A to ~1350 mg kg^{-1} in D, similar to the WP (1434 mg kg^{-1}). The DCF of downstream samples showed larger concentrations of all metal(oid)s analyzed than the DCF obtained from the WP (Table 4a). The metal(oid)s contained in the DCFs were mainly associated to the (solid) CF (1000-10 nm), i.e. minor concentrations of the elements remained in the DF, and thus the percentage of the element concentration found in the CF to that in the DCF (*CF/DCF* in Table 4a) is 100% for Fe and Al, and over 80% for the rest of analyzed elements in all soils. All metal(oid)s concentrations in the DCF from A-B-C-D decreased with distance from the WP while their fractions in the DF were low and remained constant along the river creek except for the Cu which decreased in samples C and D. For example, As concentration in the DCF decreased from 9.6 mg L^{-1} in A near

the WP, to 1.3 mg L^{-1} in D. However, As concentrations in the DF remained close to 0.2 mg L^{-1} in all samples collected along the river banks. Overall, the ratios of element concentration in DCFs to that in their corresponding bulk samples were low (2-4%) for all elements except for Al (17-31%) (Table 4a)

3.2.2. DCF size distribution and associated metal(loid)s: AF4-ICP-MS and TEM

The DCF size distribution and the associated As, Fe, and Al contents of downstream samples were analyzed by AF4-UV-vis-ICP-MS. Low pH and high EC of WP sample prevented its size-characterization due to the strong interaction with the AF4 channel membrane (Gomez-Gonzalez et al., 2016).

The size maxima of the colloidal distributions did not change with distance along the stream over the samples A to D (Table 5). Iron and As concentration maxima were associated to colloid mean sizes of 260±30 nm and 257±36 nm, respectively, and differed little to that of Al, 263±30 nm (Table 5, Figure 2a). These size ranges were further confirmed as colloid particles 200-300 nm large were frequently observed in the DCF by TEM analyses (Figure 2b). The EDX indicated the importance of Al- and Fe-bearing phases in the As mobilization (Table S5).

3.2.3. Colloidal Arsenic and Fe XAS speciation

The As K-edge EXAFS spectra acquired over the CF (1000-10 nm) of the samples pointed to ferrihydrite [$Fe_{10}O_{14}(OH)_2$] as the main As-bearing phase in downstream samples (Table 3, Figure 1), accompanied by low contributions of goethite [α-FeO(OH)] in A and B, beudantite [$PbFe_3(OH)_6\,SO_4\,AsO_4$] in C, and jarosite in D. In the WP, in addition to ferrihydrite and goethite, there was a significant contribution of scorodite (≈36%).

The Fe k-edge EXAFS spectra showed similar Fe-clays in the colloidal fraction of all samples. In the WP there were similar contributions of smectite [$Ca_{0.17}$(Al, Fe, Mg)$_2$(Si, Al)$_4O_{10}(OH)_2 \cdot nH_2O$], schwertmannite [$Fe_8O_8(OH)_6(SO_4) \cdot nH_2O$] and plumbo-jarosite [$PbFe_6(SO_4)_4(OH)_{12}$]. All A-B-C zones showed the main presence of schwertmannite in the CF and minor contributions of Fe-phyllosilicates (smectite and illite [(K, H_3O)(Al, Mg, Fe)$_2$(Si, Al)$_4O_{10}$[(OH)$_2$, H_2O]]) and (plumbo)jarosite (Table 3, Figure 1).

4. DISCUSSION

4.1. Arsenic spreading and environmental impact

The massive sulfarsenide residues dumped on the soil surface near the creek are an important source of metal(oid) contamination in the mine surroundings, especially downstream. At about one kilometer downstream from the WP, As concentration is 43 times higher than the regional legal threshold (24 mg kg^{-1}, Moreno-Jimenez et al. 2009). Primary As-bearing mineral assemblages, mainly pyrite-like minerals, are transformed to authigenic minerals such as goethite and scorodite, the main products of low-temperature meteorization of the WP, and minor fractions of jarosite, plumbojarosite, and schwertmannite. Atmospheric oxidation of pyrite begins within minutes of exposure, resulting in the production of Fe-oxyhydroxides and sulfate species (Chandra and Gerson, 2010). The extent of oxidation is naturally controlled by access of mine wastes to oxygenated water, which is enhanced by specific geographical characteristics of the area such as its high topographic relief, and alternation of dry and wet climate (Majzlan et al., 2014). The microbial activity may also play a significant role in As-bearing mineral dissolution and As transformations in the soil-water system (Lloyd and Oremland, 2006).

297 This process is confirmed by EXAFS, indicating that As is only present as As(V) in
298 both WP and downstream samples (Table 3). Fe-Mössbauer spectroscopy shows major
299 proportions of structural Fe(III) over Fe(II) indicating the high oxidation state at the
300 surface of the originally pyritic wastes (Table 2). Furthermore, As partitioning in the
301 solid phase of the WP samples shows the largest proportion of As bound to poorly
302 crystalline Fe-oxyhydroxide minerals (Fraction IV, 74%), and no As is associated to the
303 most bioavailable or soluble fraction (Table S4). Similar to Slowey et al. (2007), no
304 primary minerals were detected in the mobilizable CF in the WP and samples
305 downstream.
306 The lower As total concentration downstream (Table 1), relative to that in the WP, is the
307 result of geochemical mechanisms that constrain the As release into water. Arsenic(V)
308 association to Fe-(hydr)oxides may be found in the WP in either large particles or
309 strongly-bound colloidal aggregates with limited dispersibility. Thus, reduced amounts
310 of As travel downstream from the WP relative to the large As pool in the WP. Although
311 no reclamation has been performed in the residues and affected soils, acid release from
312 pyrite oxidation is neutralized along the creek to circumneutral values due to
313 endogenous calcite hosted in neighboring granite and the existence of hidden
314 interstratified marble banks into the gneiss series. At pH>6, ferrihydrite formation is
315 favorable (Hayes et al., 2014) and can exert a metal trapping role (Fritzsche et al., 2011)
316 attenuating As toxicity. The sequential extractions also indicate an increasing proportion
317 of As coprecipitation with crystalline Fe-oxyhydroxides in soil samples with distance
318 from the WP (Table S4) consistent with the As retention through stable inner-sphere
319 complexes.
320 However, our results show a remarkable metal(oid) pollution of the soil-water system in
321 the area. Thus, sorption onto mineral phases at the source does not prevent the release

and transport of As and other metals. One potential mechanism is the transport of colloid-size reactive particles rich in As and the subsequent downstream spreading of the element (Bauer and Blodau, 2009). Even though As concentration in the DCF represents approximately 3% of total As concentration in the samples (Table 4) this fraction might justify the contamination downstream over time taking into account that at the circumneutral pH of the running water and soil samples (Table 1), minor concentrations of As are encountered as truly dissolved. Subsequent organic acid-promoted dissolution or seasonal reductive dissolution of Fe-oxyhydroxides containing As(V) (Slowey et al., 2007) may release As in fresh water. Accordingly, both bulk and colloidal As concentrations in soils decrease with distance while As concentration in stream water tend to increase downstream.

4.2. The potential role of composite mineral vectors in As transport.

Iron oxides play a role as both attenuating phases and geochemical carriers of As and metals in soil-water systems. Both mechanisms may coexist and the extent of each one depends on the concentration and transport behavior of the carrier phase, the carrier-contaminant association, and on particle settling and deposition processes in riverine systems (Hassellöv and von der Kammer, 2008). According to EXAFS, As-colloidal mobilization from the WP can be conducted by three potential carriers: ferrihydrite (or a mixture of it with schwertmannite), scorodite and goethite (Table 3). Among them, ferrihydrite is the largest contributor due to its high affinity for As(V) under oxic conditions (Dixit and Hering, 2003) and its prompt formation and stability at neutral pH values (Hayes et al., 2014). Ferrihydrite is the first metastable Fe phase to precipitate upon pyrite oxidation. Its transformation kinetics is retarded in sulfate-rich semi-arid environments. This allows this phase to persist over decades of weathering, even at

lower pHs than those predicted in its stability field (Hayes et al., 2014), although other phases such as schwertmannite are more stable at acid conditions. At pH<4, schwertmannite is an important host mineral for As released by acid mine-drainage (Acero et al., 2006), while at pH>5 sorption of As on ferrihydrite or poorly crystalline Fe-oxyhydroxide predominates (Carlson et al., 2002). The nanocrystalline structure of schwertmannite (Fernandez-Martinez et al., 2010) is corroborated by the fact that this phase is only detected by Fe-EXAFS in the CF (Table 3). Also, the high TOC (Table S1) of the samples downstream might explain its occurrence at pH>5 and the absence of As bound to schwertmannite as described by Vithana et al. (2014). Moreover, nanosized schwertmannite might have been transported as suspended material downstream as suggested by Yu et al. (1999) who also found traces of this mineral at pH>6.

Scorodite is only detected in the <2 mm and colloid fractions of the WP sample. Although this mineral is mobilizable through surface runoff (Gomez-Gonzalez et al., 2016), at neutral pH, it dissolves incongruently forming Fe-hydroxide and arsenate oxyanions (Harvey et al., 2006) and thus contributes to the accumulation of Fe-phases, which subsequently may sequester soluble As. The role of goethite as potential As-carrier seems secondary as compared to ferrihydrite. It was found in the WP colloid-size fraction (Table 3) and reduced contributions in the closest sampling points to the wastes (A and B). Ferrihydrite slowly transforms to more thermodynamically stable goethite in the presence of As (Ford, 2002). This could explain the increasing contribution of As bound to goethite in the total soil fraction with distance from the WP (Table 3), suggesting that As-bound goethite may be found in particles larger than the DCF. Nevertheless, Mössbauer spectroscopy conducted at room temperature suggests the only presence of goethite in the WP. The contribution of phases such as ferrihydrite or

371 lepidocrocite could not be discarded unless a significant number of Mössbauer spectra
372 were acquired at low temperature.
373 Although our results show the role of ferrihydrite as the main As-sorbing mineral in the
374 bulk samples, colloidal As concentration represents less than 3% of the total As
375 concentration in all samples. This indicates that ferrihydrite is mainly encountered as
376 coating or within bigger size aggregates, and in both cases with less reactivity and more
377 stability than in its nano-sized form, which likely limits its transformation to more
378 crystalline phases. Pure Fe-oxide minerals are positively charged under environmental
379 pH conditions and thus, are promptly deposited on the generally negatively charged
380 surface of stationary grains (e.g., clays) in soils and sediments (Hassellöv and von der
381 Kammer, 2008).
382 This points out the potential role of composite Fe-oxyhydroxides and phyllosilicate
383 mineral vectors as element carriers in riverine soil-water systems, acting as mineral
384 assemblages as described by Grosbois et al. (2011). The proposed mechanism would be
385 for As being attached to Fe-oxyhydroxide phases, which in turn use clays as an effective
386 physical transport media. Moreover, this role is performed regardless of the carrier
387 mineral particle size, although there is a slight enrichment in As bound to ferrihydrite in
388 the colloid-size fraction as compared to that of total soil fraction (>2mm). This is
389 supported by the fact that colloidal As mean peak size matches up with that of Fe and
390 Al in the AF4-fractograms (Figure 2) suggesting that both elements are linked to As.
391 Comparing the element's total concentrations and those found in the DCF and CF
392 (Table 4a), it is evident that the DCF becomes enriched in Al (20% or higher) while the
393 rest of the analyzed elements are present in minor proportions relative to their bulk total
394 concentrations. While the term, 'nanovector' (Hamon et al. 2005) describes the colloidal

transport of metal(oid)s in soil-water systems, it may be composed of more than one type of mineral phases for metal(oid) pollution in mine affected soil-water systems.

5. CONCLUSIONS

This work shows a potential mechanism of metal(loid) dispersion from mine wastes to adjacent soils and stream waters via long-distance transport of colloidal material. The well-known role of Fe-oxyhydroxide phases as As scavenger may be limited when they precipitate as surface coatings of dispersible colloid-size mineral particles that can readily be transferred along water courses from point sources of contamination to adjacent non-polluted sites.

The study was performed on the bulk (<2 mm) soils and their dispersible colloidal fractions (<1000 nm) combining sequential chemical extractions, fractionation and spectrometry techniques, and showed that the dispersion occurs by isolated Fe-oxyhydroxide colloids or by greater size, stable aggregates of Fe-oxyhydroxide-clay mineral composite vectors. This mobilization mechanism and the physical carrier mineral phases can be identified by combining XAS (to confirm As-Fe oxide binding) and fractionation and elemental analysis (AF4-ICP-MS).

The unlimited As source provided by the accumulation of pyrite-rich mine residues along with the decades-long mobilization of toxic elements into stream water (and its potential transfer to subsurface water) pose important risks for human health. High contents of negatively-charged clay minerals may also contribute to cationic metal-bound colloid mobilization along streams.

ACKNOWLEDGEMENTS

The Spanish Ministry of Economy and Competitiveness supported this study (CGL2010-17434). M.A. Gomez-Gonzalez was supported by the Ph.D. Spanish FPI fellowship (BES-2011-046461, EEBB-I-15-09807). XAS measurements on BM25A beamline (ESRF) supported by 25-01-944 project. ICP analyses were performed at *Servicio General de Apoyo a Investigación-SAI, Universidad-Zaragoza*. TEM analyses were performed at *Centro Nacional de Microscopía Electrónica (Universidad-Complutense, Madrid)*. ESEM-EDX and DRX analyses were performed at *MNCN-CSIC*.

FIGURE CAPTIONS

1– Arsenic K-edge EXAFS spectra of (a) bulk samples and (b) colloidal fractions. Iron K-edge EXAFS spectra of (c) colloidal fractions. Black lines, experimental data; red lines, LCF results (Table 3 for LCF values).

2– (a) AF4-ICP-MS analyses of the downstream DCFs showing the distribution of aluminum (black), iron (red) and arsenic (blue) associated to the colloids. (b) TEM images of the DCF isolated from A, B, C and D (EDX analyses confirmed the presence of As associated to Fe-oxyhydroxides in all cases (Table S5)).

REFERENCES

Acero, P., Ayora, C., Torrento, C., Nieto, J.M. 2006. The behavior of trace elements during schwertmannite precipitation and subsequent transformation into goethite and jarosite. Geochimica et Cosmochimica Acta 70, 4130-4139

Baalousha, M., Stolpe, B., Lead, J.R., 2011. Flow field-flow fractionation for the analysis and characterization of natural colloids and manufactured nanoparticles in environmental systems: A critical review. Journal of Chromatography A 1218, 4078-4103.

445 Bauer, M., Blodau, C., 2009. Arsenic distribution in the dissolved, colloidal and
446 particulate size fraction of experimental solutions rich in dissolved organic matter and
447 ferric iron. Geochimica et Cosmochimica Acta 73, 529-542.
448 Bolea, E., Laborda, F., Castillo, J.R., 2010. Metal associations to microparticles,
449 nanocolloids and macromolecules in compost leachates: Size characterization by
450 asymmetrical flow field-flow fractionation coupled to ICP-MS. Analytica Chimica Acta
451 661, 206-214.
452 Carlson, L., Bigham, J.M., Schwertmann, U., Kyek, A., Wagner, F., 2002. Scavenging
453 of As from Acid Mine Drainage by Schwertmannite and Ferrihydrite: A Comparison
454 with Synthetic Analogues. Environmental Science & Technology 36, 1712-1719.
455 Chandra, A.P., Gerson, A.R., 2010. The mechanisms of pyrite oxidation and leaching:
456 A fundamental perspective. Surface Science Reports 65, 293-315.
457 Chen, N., Jiang, D.T., Cutler, J., Kotzer, T., Jia, Y.F., Demopoulos, G.P., Rowson, J.W.,
458 2009. Structural characterization of poorly-crystalline scorodite, iron(III)–arsenate co-
459 precipitates and uranium mill neutralized raffinate solids using X-ray absorption fine
460 structure spectroscopy. Geochimica et Cosmochimica Acta 73, 3260-3276.
461 Courtin-Nomade, A., Waltzing, T., Evrard, C., Soubrand, M., Lenain, J.F., Ducloux, E.,
462 Ghorbel, S., Grosbois, C., Bril, H., 2016. Arsenic and lead mobility: From tailing
463 materials to the aqueous compartment. Applied Geochemistry 64, 10-21.
464 Dixit, S., Hering, J.G., 2003. Comparison of Arsenic(V) and Arsenic(III) Sorption onto
465 Iron Oxide Minerals: Implications for Arsenic Mobility. Environmental Science &
466 Technology 37, 4182-4189.
467 Doucet, F.J., Lead, J.R., Santschi, P.H., 2007. Colloid–Trace Element Interactions in
468 Aquatic Systems, Environmental Colloids and Particles. John Wiley & Sons, Ltd, pp.
469 95-157.

Fernandez-Martinez, A., Timon, V., Roman-Ross, G., Cuello, G.J., Daniels, J.E., Ayora, C., 2010. The structure of schwertmannite, a nanocrystalline iron oxyhydroxysulfate. American Mineralogist 95, 1312-1322.

Ford, R.G., 2002. Rates of Hydrous Ferric Oxide Crystallization and the Influence on Coprecipitated Arsenate. Environmental Science & Technology 36, 2459-2463.

Fritzsche, A., Rennert, T., Totsche, K.U., 2011. Arsenic strongly associates with ferrihydrite colloids formed in a soil effluent. Environmental Pollution 159, 1398-1405.

Gomez-Gonzalez, M.A., Voegelin, A., Garcia-Guinea, J., Bolea, E., Laborda, F., Garrido, F., 2016. Colloidal mobilization of arsenic from mining-affected soils by surface runoff. Chemosphere 144, 1123-1131.

Grosbois, C., Courtin-Nomade, A., Robin, E., Bril, H., Tamura, N., Schäfer, J., Blanc, G., 2011. Fate of arsenic-bearing phases during the suspended transport in a gold mining district (Isle river Basin, France). Science of The Total Environment 409, 4986-4999.

Hamon, R., Batley, G.E., Casey, P., 2005. Environmental nanovectors: an emerging science area. SETAC Globe 6, 21-22.

Harvey, M.C., Schreiber, M.E., Rimstidt, J.D., Griffith, M.M., 2006. Scorodite Dissolution Kinetics: Implications for Arsenic Release. Environmental Science & Technology 40, 6709-6714.

Hassellöv, M., von der Kammer, F., 2008. Iron Oxides as Geochemical Nanovectors for Metal Transport in Soil-River Systems. Elements 4, 401-406.

Hayes, S.M., Root, R.A., Perdrial, N., Maier, R.M., Chorover, J., 2014. Surficial weathering of iron sulfide mine tailings under semi-arid climate. Geochimica et Cosmochimica Acta 141, 240-257.

494 Kretzschmar, R., Borkovec, M., Grolimund, D., Elimelech, M., 1999. Mobile
495 Subsurface Colloids and Their Role in Contaminant Transport, in: Donald, L.S. (Ed.),
496 Advances in Agronomy. Academic Press, pp. 121-193.
497 Laborda, F., Ruiz-Beguería, S., Bolea, E., Castillo, J.R., 2011. Study of the size-based
498 environmental availability of metals associated to natural organic matter by stable
499 isotope exchange and quadrupole inductively coupled plasma mass spectrometry
500 coupled to asymmetrical flow field flow fractionation. Journal of Chromatography A
501 1218, 4199-4205.
502 Lloyd, J.R., Oremland, R.S., 2006. Microbial transformations of arsenic in the
503 environment: From Soda lakes to aquifers. Elements 2, 85-90.
504 Maddock, A.G., 1985. Mössbauer Spectrometry in Mineral Chemistry. Chemical
505 Bonding and Spectroscopy in Mineral Chemistry In: F.J. Berry and D.J. Vaughan, eds.
506 Springer Netherlands, 141-208.
507 Majzlan, J., Drahota, P., Filippi, M., 2014. Parageneses and Crystal Chemistry of
508 Arsenic Minerals. Reviews in Mineralogy and Geochemistry 79, 17-184.
509 Medrano, M.J., Boix, R., Pastor-Barriuso, R., Palau, M., Damián, J., Ramis, R., del
510 Barrio, J.L., Navas-Acien, A., 2010. Arsenic in public water supplies and cardiovascular
511 mortality in Spain. Environmental Research 110, 448-454.
512 Moreno-Jiménez, E., Peñalosa, J.M., Manzano, R., Carpena-Ruiz, R.O., Gamarra, R.,
513 Esteban, E., 2009. Heavy metals distribution in soils surrounding an abandoned mine in
514 NW Madrid (Spain) and their transference to wild flora. Journal of Hazardous Materials
515 162, 854-859.
516 Neubauer, E., von der Kammer, F., Knorr, K.H., Peiffer, S., Reichert, M., Hofmann, T.,
517 2013. Colloid-associated export of arsenic in stream water during stormflow events.
518 Chemical Geology 352, 81-91.

519 O'Day, P.A., Vlassopoulos, D., Root, R., Rivera, N., 2004. The influence of sulfur and
520 iron on dissolved arsenic concentrations in the shallow subsurface under changing redox
521 conditions. Proceedings of the National Academy of Sciences of the United States of
522 America 101, 13703-13708.
523 Plathe, K.L., von der Kammer, F., Hassellöv, M., Moore, J., Murayama, M., Hofmann,
524 T., Hochella, M.F., 2010. Using FlFFF and aTEM to determine trace metalnanoparticle
525 associations in riverbed sediment. Environmental Chemistry 7, 82-93.
526 Ravel, B., Newville, M., 2005. ATHENA, ARTEMIS, HEPHAESTUS: data analysis
527 for X-ray absorption spectroscopy using IFEFFIT. Journal of Synchrotron Radiation 12,
528 537-541.
529 Serrano, S., Gomez-Gonzalez, M.A., O'Day, P.A., Laborda, F., Bolea, E., Garrido, F.,
530 2015. Arsenic speciation in the dispersible colloidal fraction of soils from a mine-
531 impacted creek. Journal of Hazardous Materials 286, 30-40.
532 Slowey, A.J., Johnson, S.B., Newville, M., Brown Jr, G.E., 2007. Speciation and colloid
533 transport of arsenic from mine tailings. Applied Geochemistry 22, 1884-1898.
534 Villalobos, M., García-Payne, D.G., López-Zepeda, J.L., Ceniceros-Gómez, A.E.,
535 Gutiérrez-Ruiz, M.E., 2010. Natural Arsenic Attenuation via Metal Arsenate
536 Precipitation in Soils Contaminated with Metallurgical Wastes: I. Wet Chemical and
537 Thermodynamic Evidences. Aquatic Geochemistry 16, 225-250.
538 Vithana, C.L., Sullivan, L.A., Burton, E.D., Bush, R.T., 2014. Liberation of acidity and
539 arsenic from schwertmannite: Effect of fulvic acid. Chemical Geology 372, 1-11.
540 Voegelin, A., Weber, F.-A., Kretzschmar, R., 2007. Distribution and speciation of
541 arsenic around roots in a contaminated riparian floodplain soil: Micro-XRF element
542 mapping and EXAFS spectroscopy. Geochimica et Cosmochimica Acta 71, 5804-5820.

543 Yu, J-Y., Heo, B., Choi, I-K., Cho, J-P., Chang. H-W., 1999. Apparent solubilities of
544 schwertmannite and ferrihydrite in natural stream waters polluted by mine drainage.
545 Geochimica et Cosmochimica Acta, 63, 3407–3416.

546

547

Table 1 – Elemental concentrations of soil/sediment and stream waters

Soil/sediment	Al	Mn	Fe	Cu	Zn	As	Pb	As/Fe [b]
	mg kg^{-1} [a]							
WP	1550	364	6.9x10^4	369	365	2.2x10^4	3213	0.23
A	4120	957	3.4x10^4	1886	1525	3313	448	0.07
B	2930	838	2.3x10^4	1383	1172	2278	354	0.07
C	2440	668	2.1x10^4	360	1331	816	172	0.03
D	2140	467	1.9x10^4	281	1167	1041	182	0.04

Stream waters	pH [c]	EC *μS cm^{-1}*	Mn	Fe	As	Pb
			μg L^{-1} [d]			
WP	3.92	237	204±8.8	250±31	32±1.7	14±0.3
A	6.88	49.7	7.1±0.8	60±10	67±6.1	0.52±0.06
B	7.01	46.0	2.8±0.1	90±17	92±11	0.88±0.03
C	6.90	47.8	1.7±0.2	69±8.9	108±10	0.75±0.03
D	7.23	47.3	1.8±0.4	56±4.8	87±2.2	0.24±0.01

[a] Pseudo-total concentrations of soils were measured by ICP-OES after aqua-regia addition and microwave-assisted digestion. Standard deviations of the ICP-OES determinations for each analyzed element are: Al = ± 13.1 mg kg^{-1}, Mn = ± 1.2 mg kg^{-1}, Fe = ± 7.2 mg kg^{-1}, Cu = ± 0.7 mg kg^{-1}, Zn = ± 1.0 mg kg^{-1}, As = ± 0.3 mg kg^{-1}, Pb = ± 2.4 mg kg^{-1}

[b] Arsenic/Iron molar ratio

[c] pH and electrical conductivity (EC) of stream samples were also analyzed

[d] Pseudo-total concentrations of stream waters were measured by ICP-MS after aqua-regia addition and microwave-assisted digestion. Standard deviations (n=3) are presented in the table

Table 2 – Relative areas of the different components identified in the Mössbauer spectra

Sample	Fe(III) doublet	Fe(II) doublet	Fe(III) hematite	Fe(III) goethite	Fe(II)/ Fe(III) [a]
	%				
WP	81	3		16	0.03
A	88	12			0.14
B	79	21			0.27
C	64	17	19		0.20
D	63	15	22		0.18

[a] Fe(II)/Fe(III) molar ratio after fitting the areas of the Mössbauer spectra

Table 3 – Linear combination fit results for As and Fe K-edge EXAFS spectra of soil/sediments and CF samples

Soil/sediment - As EXAFS [a]							
Sample	**As-FH [b]**	**Scorodite**	**As-Jar [c]**	**As-Goe [d]**	**Total**	**R factor [e]**	**red χ^{2} [f]**
	%						
WP	56.0	26.2	16.9		99.1	0.010	0.171
A	97.3			1.6	98.9	0.014	0.330
B	70.5			23.1	93.6	0.021	0.487
C	85.8			11.0	96.8	0.021	0.489
D	70.7			22.1	92.8	0.052	1.08

CF - As EXAFS [a]								
Sample	**As-FH [b]**	**Scor.**	**As-Goe[d]**	**Beudan.**	**As-Jar [c]**	**Total**	**R factor[e]**	**red χ^{2} [f]**
	%					*(%)*		
WP	50.8	35.9	15.1			101.8	0.017	0.438
A	97.1		6.3			103.4	0.017	0.456
B	92.3		7.8			100.1	0.022	0.552
C	90.1			13.4		103.5	0.091	2.53
D	96.3				4.2	100.5	0.041	1.02

CF -Fe EXAFS [g]								
Sample	**Smectite**	**Schwert.**	**Pb-Jaros.**	**Illite**	**Jarosite**	**Total**	**R factor[e]**	**red χ^{2} [f]**
	%					*(%)*		
WP	36.2	34.2	33.9			104.3	0.008	0.100
A		57.0		26.4	16.3	110.0	0.020	0.194
B	15.6	62.9	16.0			94.5	0.006	0.058
C		58.0		26.9	20.9	105.8	0.008	0.090

[a] Linear combination fit (LCF) was applied over the k-range: 2-10.5 $Å^{-1}$ on the As-EXAFS spectra
[b] Arsenic(V) sorbed to ferrihydrite
[c] Arsenic(V) sorbed to jarosite
[d] Arsenic(V) sorbed to goethite
[e] Normalized sum of the squared residuals of the fit [$R = \sum(\text{data-fit})^2 / \sum\text{data}^2$)]
[f] Goodness-of-fit was assessed by the χ^2 statistic [= (F factor) / (no. of points – no. of variables)]
[g] Linear combination fit (LCF) was applied over the k-range: 2-7 $Å^{-1}$ on the Fe-EXAFS spectra

Table 4 – (a) Pseudo-total element concentrations of DCF and DF. (b) Colloidal mass of each DCF and their corresponding As and Fe concentrations per mass of colloid.

(a)	Sample	As	Al	Fe	Cu	Zn	Pb
		mg L^{-1} [a]					
WP	*DCF*	0.23±0.05	0.73±0.06	1.13±0.22	0.22±0.01	0.39±0.04	0.04±0.01
	DF	0.03±0.01	0.64±0.08	0.74±0.29	0.23±0.02	0.39±0.04	0.01±0.01
	CF [b]	0.20	0.09	0.39	- [c]	- [c]	0.03
	CF/DCF [d]	87%	12%	34%	0%	0%	75%
	DCF/bulk [e]	0.01%	0.5%	0.02%	0.6%	1%	0.01%
A	*DCF*	9.58±0.16	84±0.19	81±0.54	3.85±0.12	3.68±0.11	1.59±0.38
	DF	0.21±0.03	0.05±0.04	0.03±0.03	0.21±0.04	0.12±0.02	0.01±0.01
	CF	9.37	~ 84	~ 81	3.64	3.56	1.58
	CF/DCF	98%	100%	100%	95%	97%	99%
	DCF/bulk	3%	20%	2%	2%	2%	4%
B	*DCF*	7.54±0.19	68±0.21	55±0.60	4.80±0.17	4.12±0.24	1.44±0.35
	DF	0.20±0.06	0.08±0.07	0.03±0.03	0.23±0.05	0.18±0.01	0.01±0.01
	CF	7.34	~ 68	~ 55	4.57	3.94	1.43
	CF/DCF	97%	100%	100%	95%	96%	99%
	DCF/bulk	3%	23%	2%	3%	4%	4%
C	*DCF*	2.31±0.18	76±0.27	47±0.46	0.87±0.08	4.40±0.19	0.60±0.37
	DF	0.22±0.07	0.05±0.02	0.03±0.03	0.06±0.01	0.35±0.03	0.01±0.01
	CF	2.09	~ 76	~ 47	0.81	4.05	0.59
	CF/DCF	90%	100%	100%	93%	92%	98%
	DCF/bulk	3%	31%	2%	2%	3%	3%
D	*DCF*	1.29±0.21	37±0.15	24±0.31	0.46±0.16	1.92±0.07	0.32±0.21
	DF	0.23±0.07	0.06±0.05	0.03±0.03	0.04±0.01	0.18±0.02	0.01±0.01
	CF	1.06	~ 37	~ 24	0.42	1.74	0.31
	CF/DCF	82%	100%	100%	91%	91%	97%
	DCF/bulk	1%	17%	1%	2%	2%	2%

(b)	Sample	Colloids	As	Fe	As / Fe [h]
		mg kg^{-1} [f]	*mg kg coloid^{-1}* [g]		
	WP	1395 ± 313	1434	2796	0.15
	A	9206 ± 367	10178	87987	0.09
	B	7744 ± 639	9478	71021	0.10
	C	7989 ± 496	2616	58830	0.04
	D	7869 ± 488	1347	30498	0.04

[a] Pseudo-total concentrations ± standard deviations (n = 3) of the ICP-OES determinations after aqua-regia addition and microwave-assisted digestion (Soil:Ultrapure water relationship = 4g/40 mL)
[b] The concentration of the colloidal fraction (CF, 1000-10 nm) is calculated as the difference between the dispersible colloidal fraction (DCF, < 1000 nm) and the dissolved fraction (DF, < 10 nm)
[c] Most or all of the metal(loid) is present only in the DF
[d] Relative contribution of the element concentration in the colloidal fraction (CF) to that in the dispersible colloidal fraction (DCF)
[e] Relative contribution of the element concentration in the dispersible colloidal fraction (DCF) to that in the bulk concentration, after transforming the DCF concentration to mg kg^{-1}
[f] Colloidal mass calculated following the procedure described by Plathe *et al.* (2010), ± standard deviations (n = 3)
[g] Arsenic and iron concentrations in the colloidal fraction (CF, Table 9b) per kilogram of colloid
[h] Arsenic and iron molar ratio in the colloidal fraction

Table 5 – Maximum of colloidal sizes and recoveries of the DCF determined by AF4 [a]

Sample	AF4-ICP-MS					
	Al		***As***		***Fe***	
	nm [b]	*%* [c]	*nm* [b]	*%* [c]	*nm* [b]	*%* [c]
A	264	71.9	257	67.8	254	68.2
B	306	48.7	307	53.8	305	40.4
C	234	56.3	221	55.5	238	43.6
D	251	45.7	245	52.0	246	41.3

[a] The data shown are the average values of three replicates
[b] Maximum of size of the distribution found by AF4
[c] Recoveries (in percentage) obtained for the DCF analyzed

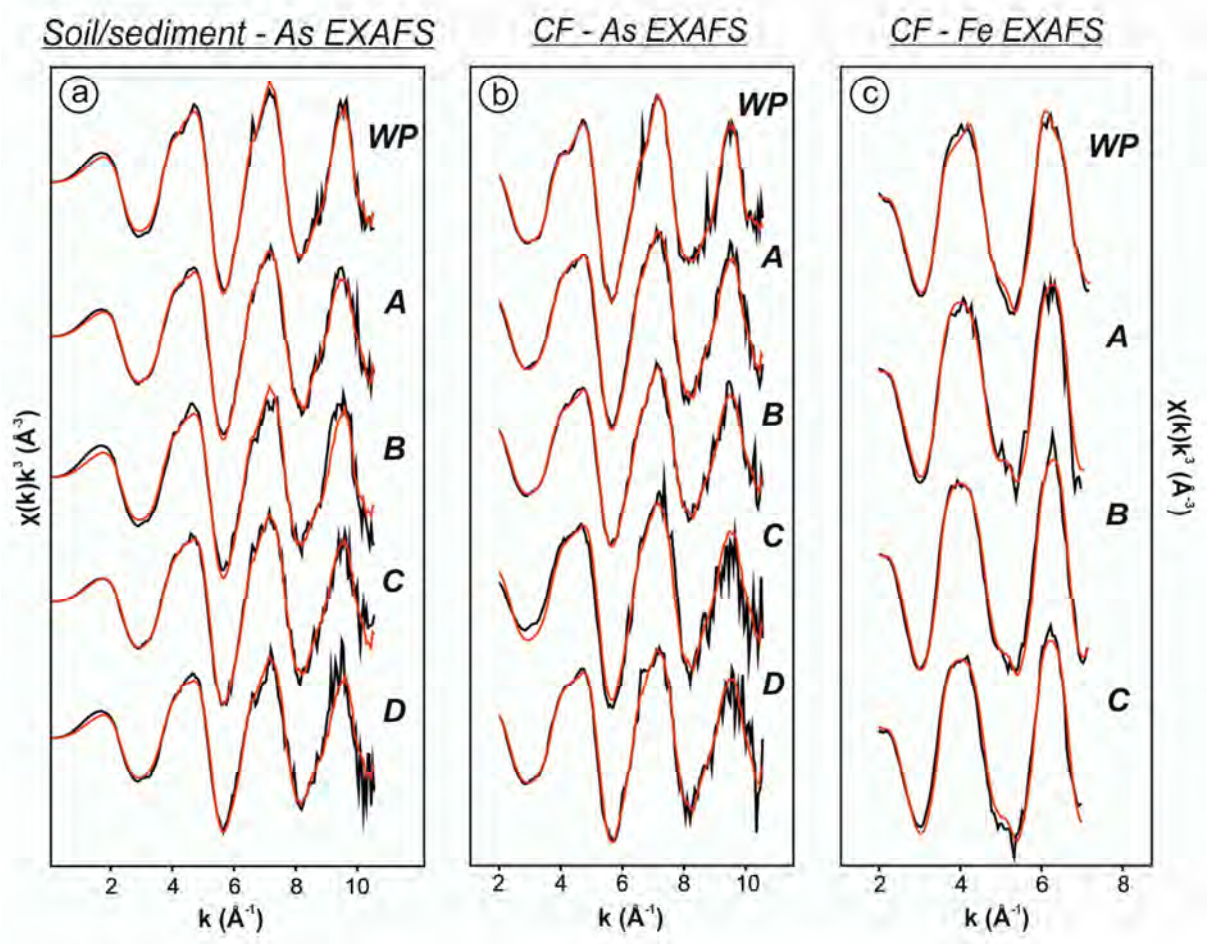

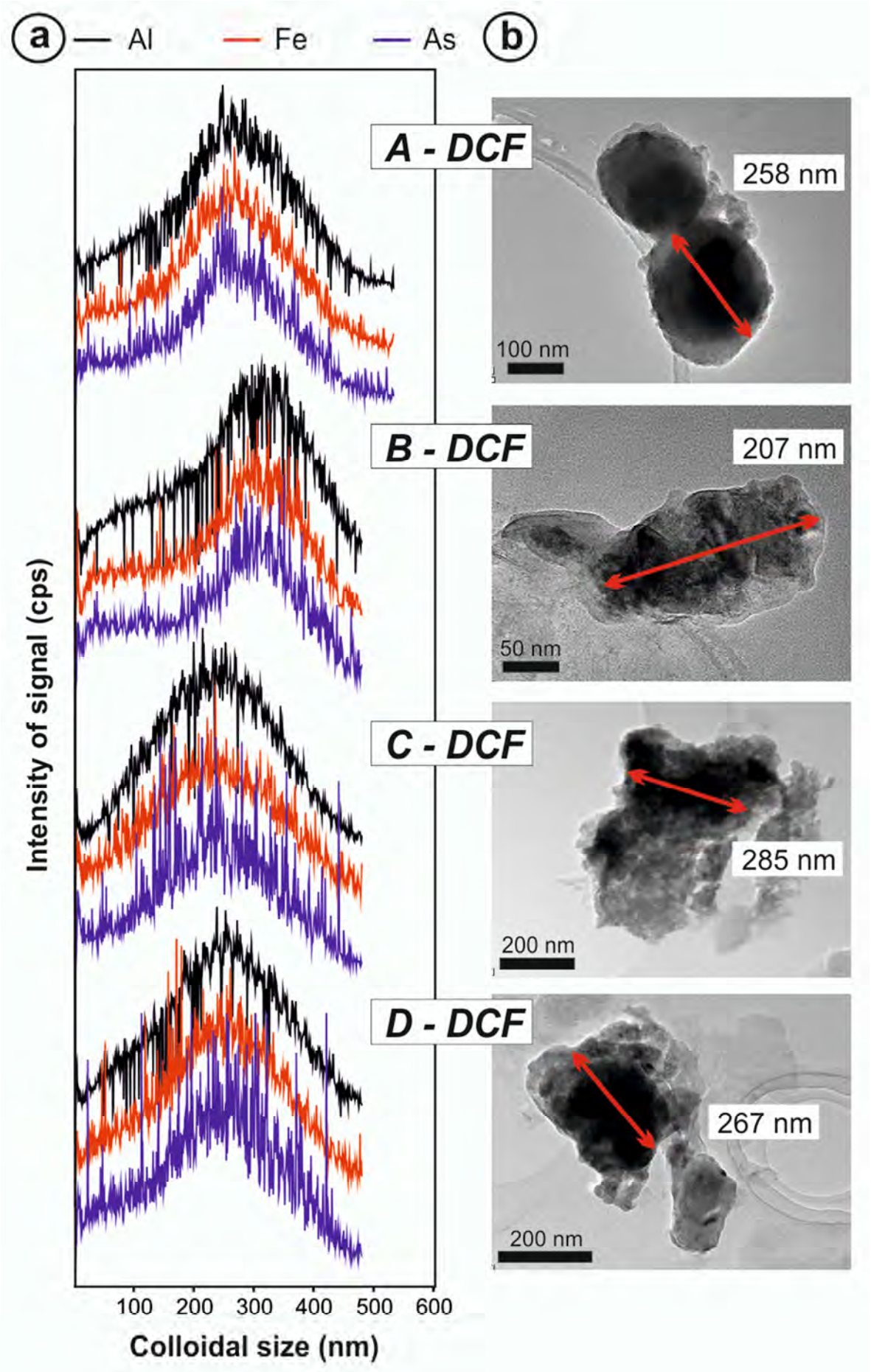
a
Al
Fe
As
b
A - DCF
B - DCF
C - DCF
D - DCF
258 nm
100 nm
207 nm
50 nm
285 nm
200 nm
267 nm
200 nm
Intensity of signal (cps)
100
200
300
400
500
600
Colloidal size (nm)

Iron oxide - clay composite vectors on long-distance transport of arsenic and toxic metals in mining-affected areas

Miguel Angel Gomez-Gonzalez[a], Mario Villalobos[b], Jose Francisco Marco[c], Javier Garcia-Guinea[a], Eduardo Bolea[d], Francisco Laborda[d], Fernando Garrido[a]

[a] *Museo Nacional de Ciencias Naturales (MNCN, CSIC). C/ Jose Gutierrez Abascal 2, 28006, Madrid, Spain.*
[b] *Instituto de Geología. Universidad Nacional Autónoma de México (UNAM), Coyoacán, D.F. 04510, Mexico.*
[c] *Instituto de Química Física-Rocasolano (CSIC), C/ Serrano 119, 28006, Madrid, Spain.*
[d] *Instituto Universitario de Ciencias Ambientales (IUCA), Universidad de Zaragoza. C/ Pedro Cerbuna 12, 50009, Zaragoza, Spain.*

HIGHLIGHTS

- Long-distance dispersion of arsenic through mobile colloids is demonstrated
- Ferrihydrite found as thin coatings on clay minerals acts as arsenic sorbing phase
- This association carries other metals in concentrations above regulatory levels
- This association limits the role of iron oxides to attenuate arsenic pollution